

## **Supporting Informations**

### **Atomic-scaled cobalt encapsulated in P,N-doped carbon sheath over carbon nanotube for enhanced oxygen reduction electrocatalysis under acid and alkaline media**

Shiyu Guo,<sup>a</sup> Pengfei Yuan,<sup>b</sup> Jianan Zhang,<sup>\*a</sup> Pengbo Jin,<sup>a</sup> Hongming Sun,<sup>c</sup> Kaixiang Lei,<sup>c</sup> Xinchang Pang,<sup>a</sup> Qun Xu,<sup>\*,a</sup> and Fangyi Cheng<sup>\*,c</sup>

<sup>a</sup>College of Materials Science and Engineering, Zhengzhou University, Zhengzhou 450001, P. R. China

<sup>b</sup>International Joint Research Laboratory for Quantum Functional Materials of Henan Province, and School of Physics and Engineering, Zhengzhou University, Zhengzhou 450001, P. R. China

<sup>c</sup>Key Laboratory of Advanced Energy Materials Chemistry (Ministry of Education), Nankai University, Tianjin 30071, P. R. China

\*Corresponding authors E-mails: zjn@zzu.edu.cn (J. N. Zhang), qunxu@zzu.edu.cn (Q. Xu), and fycheng@nankai.edu.cn (F. Y. Cheng)

## Table of Contents

1. Experimental Section
2. Supplementary Figures and Tables
3. Computational Section
4. References

## 1. Experimental Section

*Chemicals and reagents.* Multi-walled CNT (MWCNTs) was obtained from Beijing DK nano technology Co., Ltd. Cobalt nitrate hexahydrate ( $\text{Co}(\text{NO}_3)_2 \cdot 6\text{H}_2\text{O}$ ) was obtained from Beijing Chemical Reagent Company. Triphenylphosphine (TPP), melamine and ethanol were obtained from Sinopharm Chemical Reagent Co., Ltd. Ammonia and formaldehyde were obtained from Xilong Chemical Co., Ltd. Resorcinol, sulfuric acid ( $\text{H}_2\text{SO}_4$ ) and nitric acid ( $\text{HNO}_3$ ) were obtained from the Tianjin Chemical Factory. Nafion (5.0 wt%) were purchased from Sigma-Aldrich. All chemicals were used as received without any further purification. Pt catalyst (20% Pt supported on Vulcan XC-72 carbon) was obtained from Johnson Matthey. Deionized water was used in all experiments.

### *Synthesis of resorcinol-melamine-formaldehyde coated CNTs (RMF@CNT).*

RMF@CNT is prepared by polymerization of resorcinol, formaldehyde and melamine on the surface of the MWCNTs. MWCNTs were first pre-treated in a  $\text{HNO}_3/\text{H}_2\text{SO}_4$  (v/v = 1 : 3) mixed solution and refluxing at 70 °C for 2 h. The obtained solid was filtered using filter polytetrafluoroethylene membrane, and washed with deionized water until the pH of the filtrate reached 7 followed by drying in vacuum at 60 °C for 4 h. CNTs were dissolved in 20 mL of deionized water and sonication for 30 min. Then, 20 mL of ethanol, 30 mL of deionized water, and 0.25 mL of ammonia were added to the above solution at 70 °C under stirring. After 30 min, 0.37 mL of formaldehyde (37 wt%) and 275 mg resorcinol were added the mixture and stirring for another 30 min. Next, 630 mg melamine and 1.105 mL of formaldehyde were

added to the above mixture and continued stirring for 24 h, followed by hydrothermal treatment at 120 °C for 24 h. The obtained RMF@CNT were collected by centrifugation, washed with ethanol and water for several times, and dried at 60 °C.

*Synthesis of Co-P,N-CNT, PN-CNT, Co-N-CNT.* In typical synthesis, the as-prepared RMF@CNT, triphenylphosphine (TPP), and cobalt nitrate hexahydrate ( $\text{Co}(\text{NO}_3)_2 \cdot 6\text{H}_2\text{O}$ ) (mass ratio is 10:10:1) were immersed in 20 mL of deionized water and stirred for 2 h followed by sonication for 2 h. After drying in the oven at 80 °C for 24 h, the resulted powder was annealed at a rate of 5 °C  $\text{min}^{-1}$  to 800 °C under an  $\text{N}_2$  gas flow for 2 h. Afterwards, the sample was allowed to cool naturally to room temperature, named Co-P,N-CNT. Furthermore, PN-CNT and Co-N-CNT samples were obtained *via* the similar method but without  $\text{Co}(\text{NO}_3)_2 \cdot 6\text{H}_2\text{O}$  or TPP.

*Synthesis of Co-P-N@CNT.* The pre-treated MWCNTs, melamine, triphenylphosphine (TPP), and cobalt nitrate hexahydrate ( $\text{Co}(\text{NO}_3)_2 \cdot 6\text{H}_2\text{O}$ ) (mass ratio is 1:32:20:2) were immersed in 20 mL of deionized water and stirred for 2 h followed by sonication for 2 h. After drying in the oven at 80 °C for 24 h, the resulted powder was annealed at a rate of 5 °C  $\text{min}^{-1}$  to 800 °C under an  $\text{N}_2$  gas flow for 2 h and the sample was allowed to cool naturally to room temperature. Then, the as-obtained material was treated with 0.5 M  $\text{H}_2\text{SO}_4$  for 24 h. Afterwards, the mixture was centrifuged, and the solid material was washed three times with distilled water and dried under ambient condition, named Co-P-N@CNT.

*Characterizations.* The morphology of the samples was studied by transmission electron microscope (TEM, FEI Tecnai G2 20) with an accelerating voltage of 200 kV

and field-emission scanning electron microscope (FE-SEM, JEORJSM-6700F). The HAADF-STEM images were obtained by JEOL JEM-ARM200F at an accelerating voltage of 200 kV. Powder X-ray diffraction (XRD) patterns were collected using a Y-2000X-ray Diffractometer using copper K $\alpha$  radiation ( $\lambda=1.5406 \text{ \AA}$ ) at 40 kV, 40 mA. The Raman measurements were performed on a Renishaw spectrometer at 532 nm on a Reishaw Microscope System RM2000. The N<sub>2</sub> adsorption/desorption curve was determined by BET measurements using a Micromeritics ASAP 2020 surface area analyzer. The X-ray photoelectron spectroscopy (XPS) measurements were performed with an ESCA LAB 250 spectrometer using a focused monochromatic Al K $\alpha$  line (1486.6 eV) X-ray beam with a diameter of 200  $\mu\text{m}$ . The Co K-edge X-ray absorption near edge structure (XANES) and the extended X-ray absorption fine structure (EXAFS) were investigated at the BL14W1 beamline of Shanghai Synchrotron Radiation Facility (SSRF) in fluorescence mode using a fixed-exit Si(111) double crystal monochromator. The incident X-ray beam was monitored by an ionization chamber filled with N<sub>2</sub>, and the X-ray fluorescence detection was performed using a Lytle-type detector filled with Ar. The EXAFS raw data were then background-subtracted, normalized and Fourier transformed by the standard procedures with the IFEFFIT package.<sup>1</sup>

*Electrocatalytic measurement.* A CHI 760E electrochemical workstation (CH Instruments) was used to measure the electrocatalytic activities towards ORR. All the electrochemical measurements were conducted in a three-electrode configuration. The potential, measured against an Ag/AgCl electrode, was converted to the potential

versus the reversible hydrogen electrode (RHE). To prepare the working electrode, 2 mg each of the samples was dispersed in 0.99 mL ethyl alcohol and 0.01 mL of 5 wt% Nafion aqueous solution under sonication for about 30 min. Thereafter, 10  $\mu$ L of the obtained homogeneous catalyst ink was dropped onto a mirror polished glassy carbon electrode. For comparison of the ORR activity, Pt/C (20 wt%) electrode was prepared by using the same procedure. 0.1 M KOH aqueous solutions or 0.1 M HClO<sub>4</sub> aqueous solutions saturated with nitrogen/oxygen were employed as the electrolyte for ORR. Stability was examined by current-time chronoamperometry. The details for calculation of electron transferred number for ORR is given later.

*The calculation of electron transferred number for ORR.* On the basis of the RDE data, the electron transfer number per oxygen molecule for oxygen reduction can be determined by Koutechy-Levich equation:

$$\frac{1}{J} = \frac{1}{J_L} + \frac{1}{J_K} = \frac{1}{B\omega^{0.5}} + \frac{1}{J_K} \quad (1)$$

$$B = 0.62nFC_0(D_0)^{2/3}\nu^{-1/6} \quad (2)$$

$$J_K = nFkC_0 \quad (3)$$

Where  $J$  is the measured current density and  $\omega$  is the electrode rotating rate (rad s<sup>-1</sup>).  $B$  is determined from the slope of the Koutechy-Levich (K-L) plot based on Levich equation (2).  $J_L$  and  $J_K$  are the diffusion- and kinetic-limiting current densities,  $n$  is the transferred electron number,  $F$  is the Faraday constant ( $F = 96485 \text{ C mol}^{-1}$ ),  $C_0$  is the O<sub>2</sub> concentration in the electrolyte ( $C_0 = 1.26 \times 10^{-6} \text{ mol cm}^{-3}$ ),  $D_0$  is the diffusion coefficient of O<sub>2</sub> ( $D_0 = 1.93 \times 10^{-5} \text{ cm}^2 \text{ s}^{-1}$ ), and  $\nu$  is the kinetic viscosity ( $\nu = 0.01009 \text{ cm}^2 \text{ s}^{-1}$ ). The constant 0.62 is adopted when the rotation speed is expressed in rad s<sup>-1</sup>.

For the RRDE measurements, catalyst inks and electrodes were prepared by the same method as for RDE. The disk electrode was scanned at a rate of 5 mV s<sup>-1</sup>, and the ring potential was constant at 0.336 V in 0.1 M KOH or 1 V in 0.1 HClO<sub>4</sub> (vs. Ag/AgCl). The HO<sub>2</sub><sup>-</sup>% and transfer number (n) were determined by the followed equations:<sup>2</sup>

$$\text{HO}_2^- \% = 200 \times \frac{I_R / N}{I_D + I_R / N} \quad (4)$$

$$n = 4 \times \frac{I_D}{I_D + I_R / N} \quad (5)$$

where I<sub>d</sub> is disk current, I<sub>r</sub> is ring current, and N is current collection efficiency of the Pt ring. N was determined to be 0.40.

## 2. Supplementary Figures and Tables

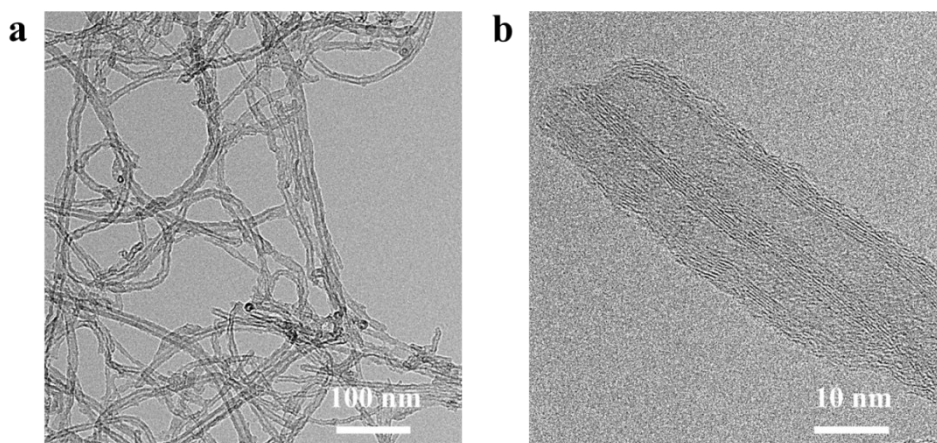


**Fig. S1.** TEM images of pre-treated CNT under different magnifications.

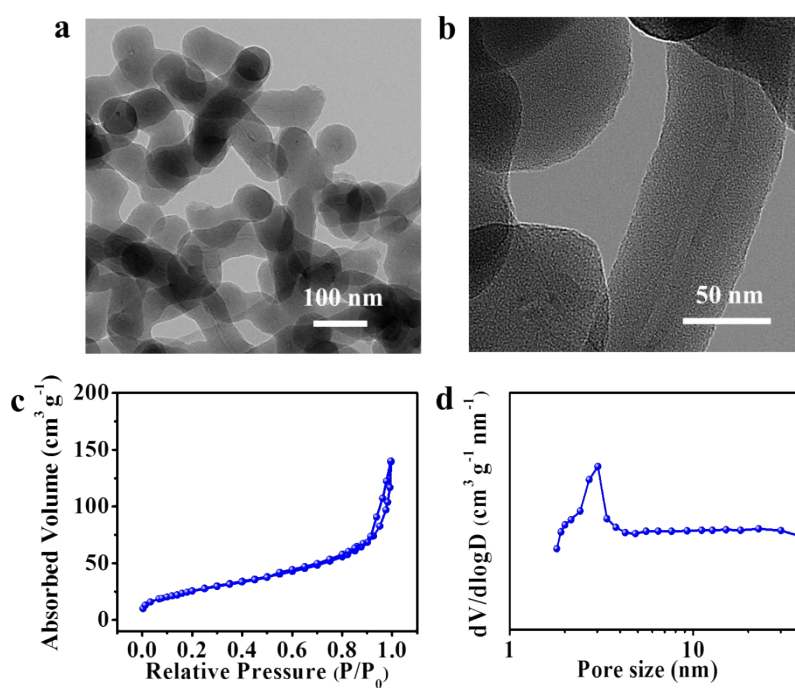


**Fig. S2.** (a,b) TEM images, (c)  $N_2$  adsorption/desorption isotherms, and (d) pore size distribution of RMF@CNT. The surface area of RMF@CNT is  $228.1 m^2 g^{-1}$ .

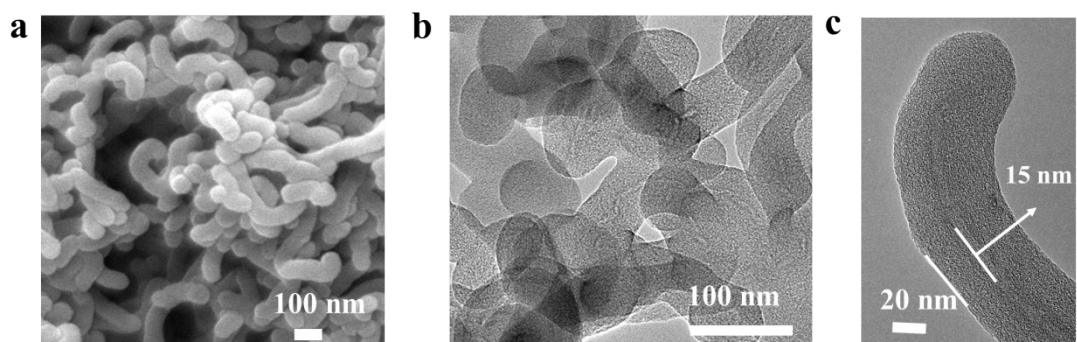


**Fig. S3.** (a) SEM image, (b) TEM image and (c) high-resolution TEM image of Co-P<sub>2</sub>N-CNT.

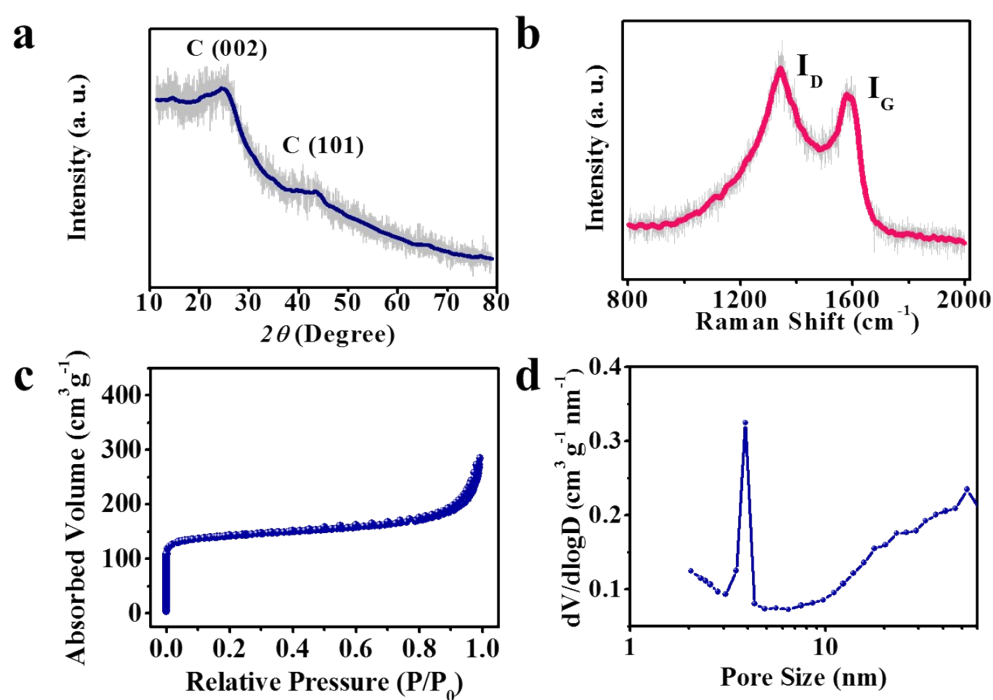


**Fig. S4.** (a) XRD pattern, (b) Raman spectrum, (c) N<sub>2</sub> adsorption and desorption isotherms and (d) pore size distribution of Co-P<sub>2</sub>N-CNT.

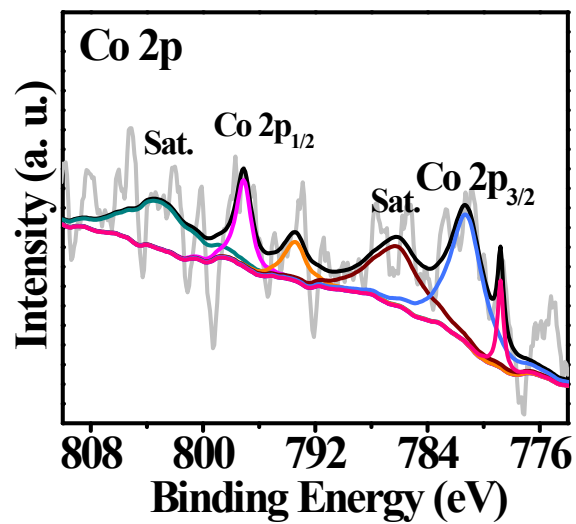


**Fig. S5.** Co 2p high-resolution XPS spectra of Co-P,N-CNT.

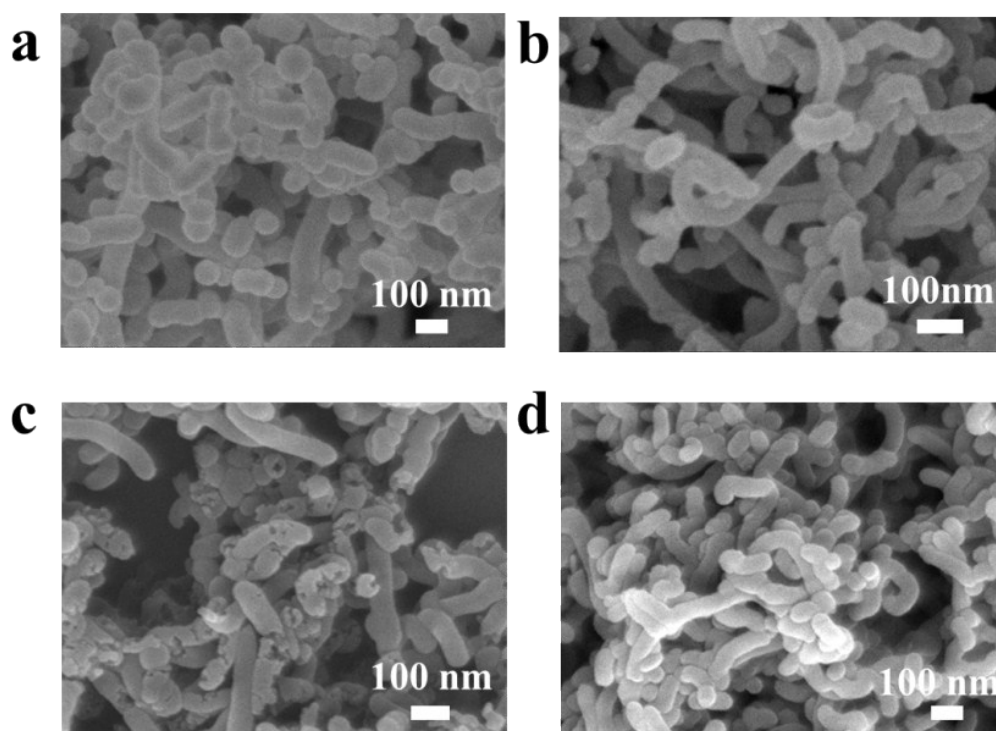


**Fig. S6.** SEM images of (a) RMF@CNT, (b) PN-CNT, (c) Co-N-CNT and (d) Co-P,N-CNT.

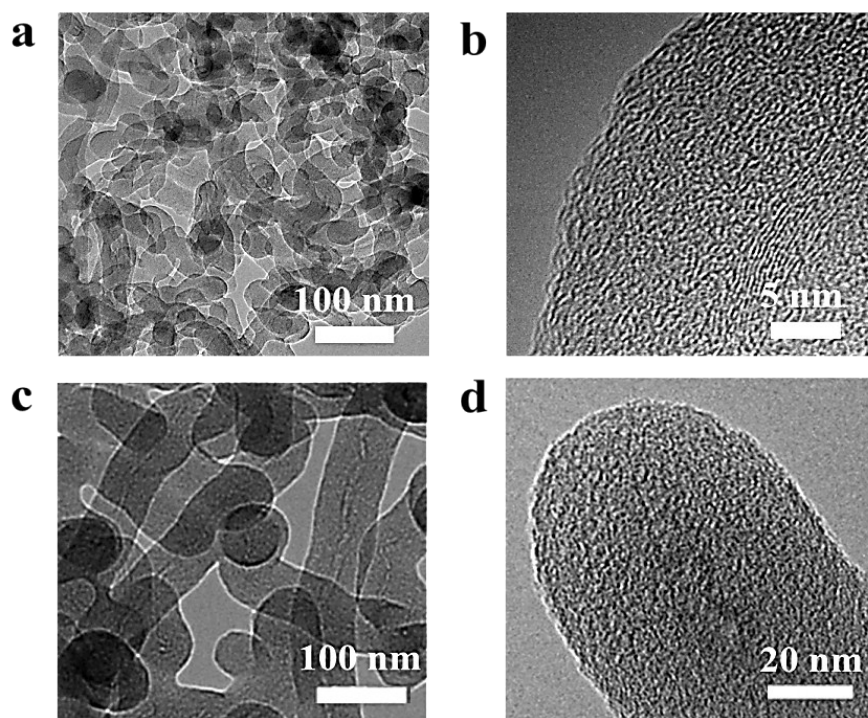


**Fig. S7.** TEM images of (a,b) PN-CNT, and (c,d) Co-N-CNT.

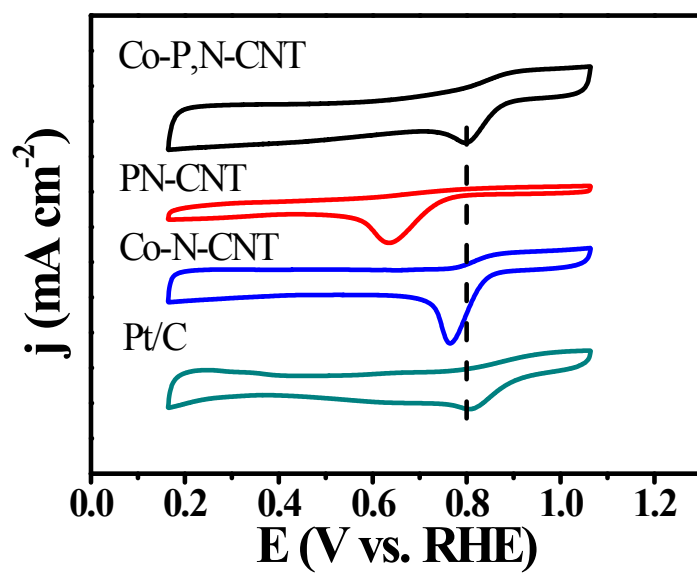


**Fig. S8.** CVs of Co-P,N-CNT, PN-CNT, Co-N-CNT and Pt/C in O<sub>2</sub>-saturated 0.1 M KOH solution at a scanning rate of 50 mV s<sup>-1</sup>.

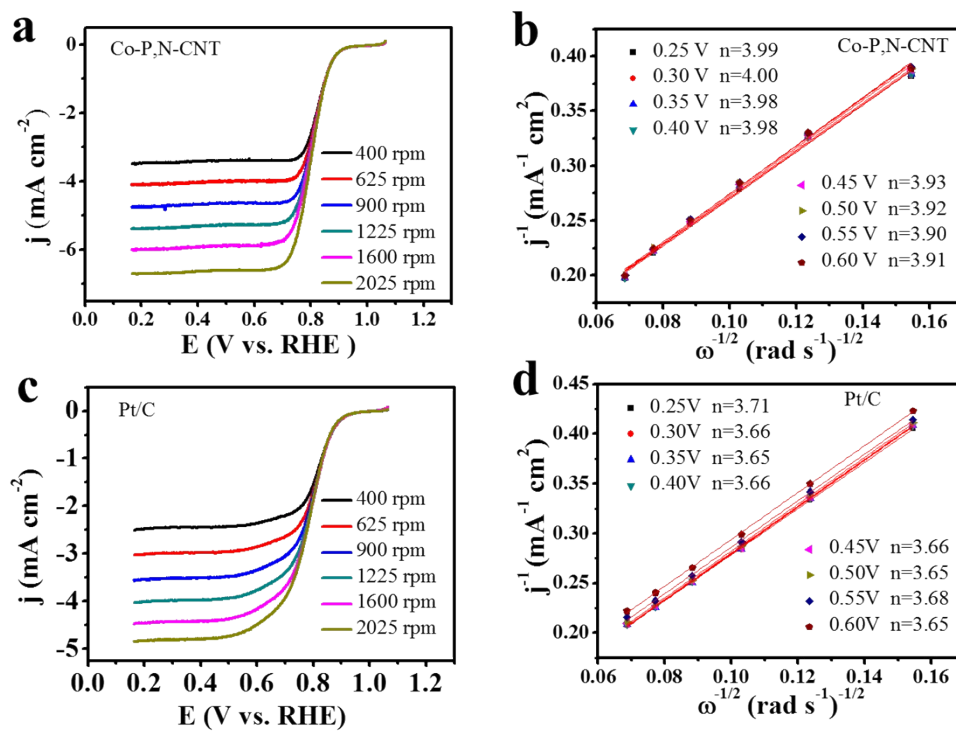


**Fig. S9.** (a,c) LSV curves at different rotation speed, (b,d) K-L plots and electron transfer number ( $n$ ) of Co-P,N-CNT and commercial Pt/C catalysts in O<sub>2</sub>-saturated 0.1 M KOH solution. Scan rate is 5 mV s<sup>-1</sup>.

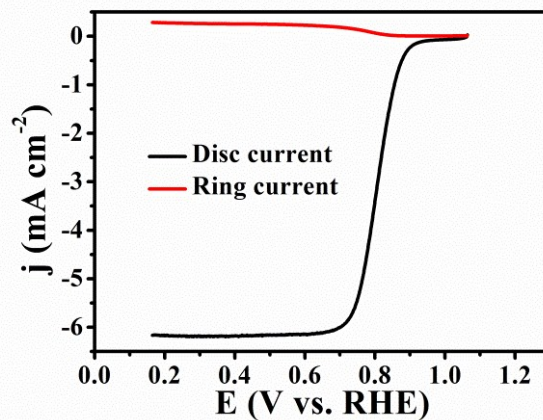


**Fig. S10.** RRDE voltammograms of Co-P,N-CNT in O<sub>2</sub>-saturated solution at a scanning rate of 50 mV s<sup>-1</sup> in 0.1 M KOH.

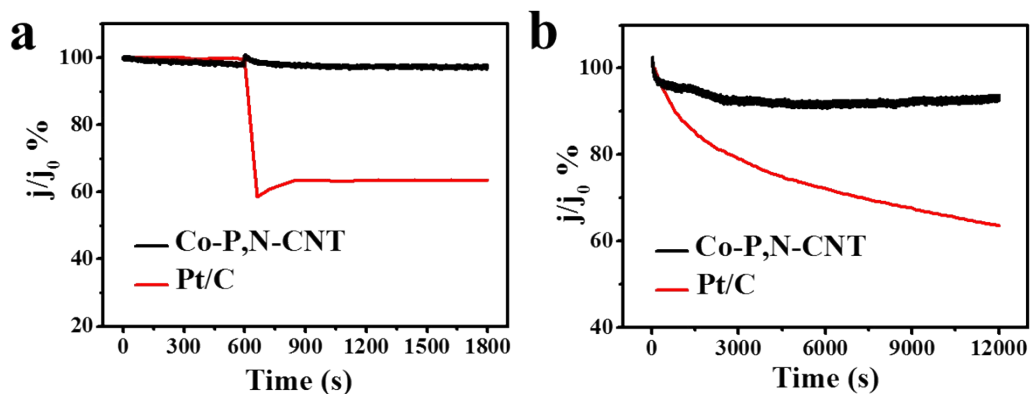


**Fig. S11.** (a) Chronoamperometric response of Co-P,N-CNT and Pt/C catalyst at 0.75 V (vs. RHE) after the introduction of 9.7 ml of CH<sub>3</sub>OH into 230.3 ml of 0.1 M KOH solution. (b) Chronoamperometric response of Co-P,N-CNT and Pt/C catalyst 0.75 V (vs. RHE) in 0.1 M KOH solution. Co-P,N-CNT exhibits a slight current decrease with 93 % retention over 12,000 s of continuous operation, whereas Pt/C exhibits a dramatic current loss with only 64 % retention

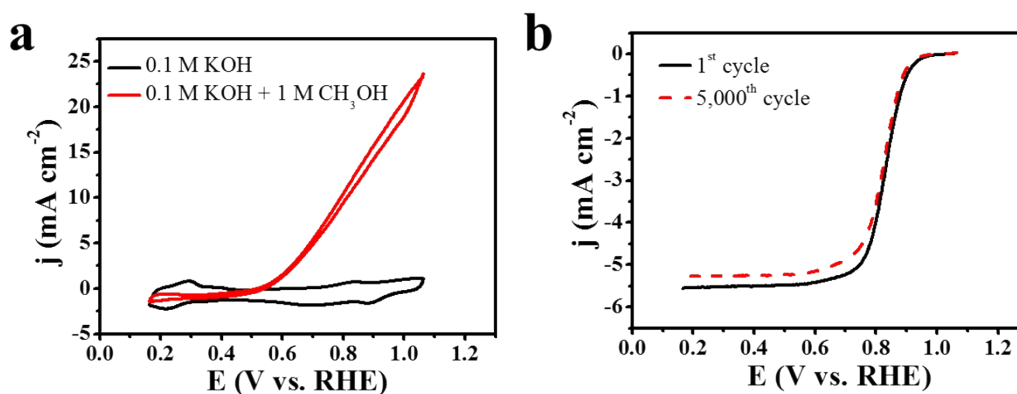


**Fig. S12.** Electrochemical methanol tolerance and durability of Pt/C. (a) CV profiles (black and red curves indicate CV curves recorded in O<sub>2</sub>-saturated 0.1 M KOH and O<sub>2</sub>-saturated 0.1 M KOH + 1 M CH<sub>3</sub>OH solution, respectively). (b) ORR polarization curves (1,600 rpm) of Pt/C before and after 5,000 cycles. Pt/C catalyst exhibits a 20 mV negative shift of the half-wave potential  $E_{1/2}$  value and also current output decrease.

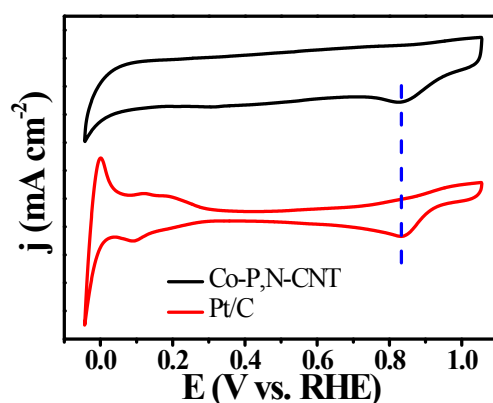


**Fig. S13.** CVs of Co-P,N-CNT and Pt/C in O<sub>2</sub>-saturated solution at a scanning rate of 50 mV s<sup>-1</sup> in 0.1 M HClO<sub>4</sub> solution. Co-P,N-CNT displays a superior ORR activity with similar cathodic reduction peak at 0.826 V to the Pt/C catalyst (0.832 V).

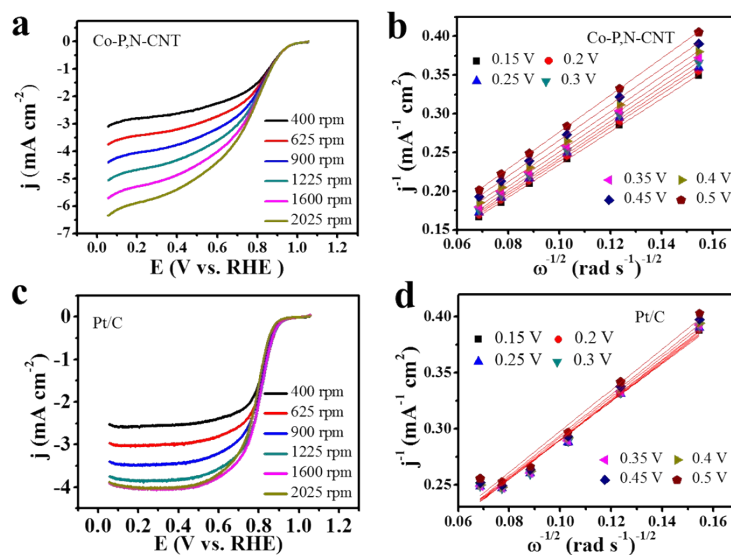


**Fig. S14.** (a,c) LSV curves, (b,d) K-L plots of Co-P,N-CNT and commercial Pt/C catalysts in O<sub>2</sub>-saturated 0.1 M HClO<sub>4</sub> solution. Scan rate is 5 mV s<sup>-1</sup>.

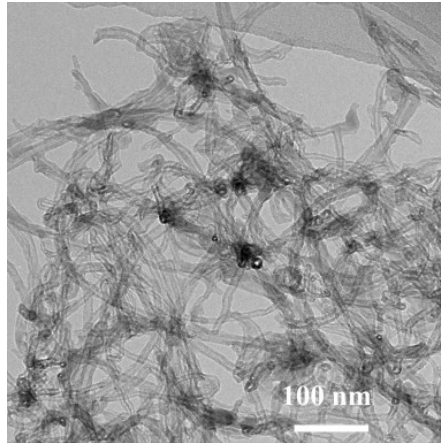


**Fig. S15.** TEM image of Co-P-N@CNT.

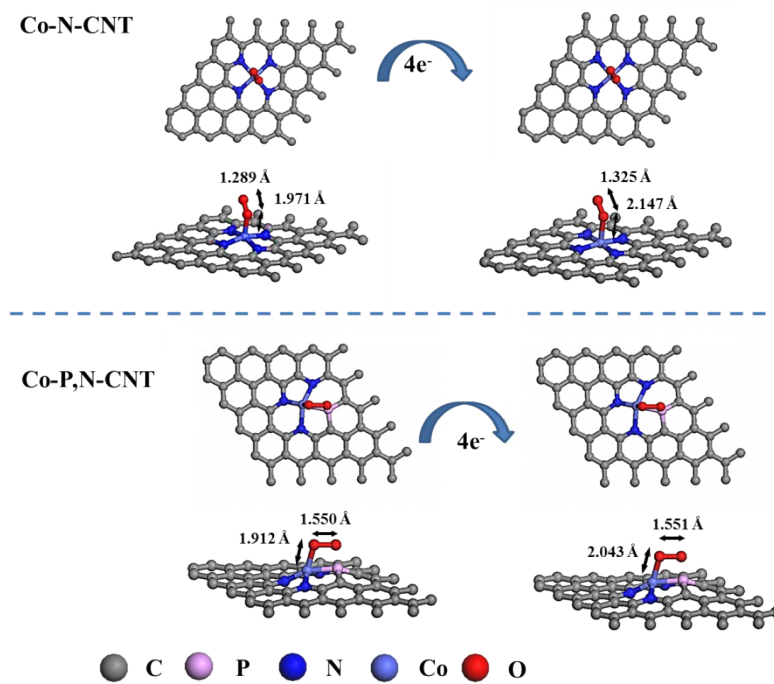


**Fig. S16.** DFT calculation on Co-N<sub>4</sub> and Co-N<sub>3</sub>P-doped graphene materials. The relaxed atomic structures of N<sub>4</sub>-Co and N<sub>3</sub>P-Co active sites by adding four charges and O<sub>2</sub>.

**Table S1.** XPS results analysis for the prepared samples. (at %)

<b>Sample Name</b>	<b>C (Atom %)</b>	<b>N (Atom %)</b>	<b>O (Atom %)</b>	<b>P (Atom %)</b>	<b>Co (Atom %)</b>
<b>Co-P,N-CNT</b>	77.94	5.36	10.04	5.64	1.02
<b>Co-N-CNT</b>	85.39	5.28	8.20		1.13
<b>PN-CNT</b>	89.95	3.52	3.38	3.15	

**Table S2.** Surface and pore related parameters from N<sub>2</sub> adsorption isotherms of samples.

<b>Sample Name</b>	<b>BET surface area (m<sup>2</sup> g<sup>-1</sup>)</b>	<b>Total pore volume (cm<sup>3</sup> g<sup>-1</sup>)</b>	<b>Micropore volume (cm<sup>3</sup> g<sup>-1</sup>)</b>	<b>Pore size (nm)</b>
<b>Co-P,N-CNT</b>	512.2	0.2	0.17	1.2/3.9/26
<b>Co-N-CNT</b>	490.9	0.2	0.20	1.3/10/52
<b>PN-CNT</b>	469.0	0.3	0.21	1.9/15/23
<b>RMF@CNT</b>	228.6	0.2	0.19	2.1/4.0/15

**Table S3.** Summary for the reported state-of-the-art transition metal/C-based ORR electrocatalysts in an alkaline medium.

Catalyst	Catalyst Loading [mg cm <sup>-2</sup> ]	Onset Potential [ $E_{\text{onsets}}$ , V]	Half-Wave Potential [ $E_{1/2}$ , V]	CV peak Potential [V]	Current density $j_L$ (mA cm <sup>-2</sup> )	Reference
<b>Co-P,N-CNT</b>	<b>0.10</b>	<b>0.916</b>	<b>0.803</b>	<b>0.798</b>	<b>5.99</b>	<b>This work</b>
Active carbon confined Mn-Co NPs	0.08	~0.864	~0.792		~4.6	[3]
<b>Porous Co-N/C hollow-carbon-sphere composites</b>	<b>0.15</b>	<b>0.950</b>	<b>0.840</b>		<b>~6.0</b>	<b>[4]</b>
Co-C NPs aligned on wrinkles of N-doped carbon	0.10	0.940	0.830	0.82	~4.5	[5]
<b>Co/N/O tri-doped graphene mesh</b>	<b>0.25</b>		<b>~0.700</b>	<b>~0.75</b>	<b>~4.8</b>	<b>[6]</b>
Cu(I)-N embedded in graphene	0.30		~0.800		~6.6	[7]
<b>Co-C<sub>3</sub>N<sub>4</sub> complexes.</b>	<b>0.40</b>	<b>~0.900</b>	<b>0.840</b>		<b>~5.3</b>	<b>[8]</b>
Co-N/C complexes	0.40	~0.900	~0.850		~5.1	[9]
Encapsulated Ni NPs N-doped hollow carbon	0.18	1.004	0.774	0.82	~4.7	[10]

**Note:** The ORR measurements were conducted in O<sub>2</sub>-saturated 0.1 M KOH solution with the rotation speed of 1600 rpm, and all  $E_{1/2}$  values were versus RHE.

**Table S4.** Summary for the reported state-of-the-art non-precious metal carbon-based ORR electrocatalysts in an acidic medium.

Catalyst	Electrolyte	Catalyst Loading [mg cm <sup>-2</sup> ]	Half-Wave Potential [ $E_{1/2}$ , V vs RHE]	Current density $j_L$ (mA cm <sup>-2</sup> )	Reference
Co-P,N-CNT	0.1 M HClO <sub>4</sub>	0.10	0.78	5.6	This work
Porous Co-N/C hollow-carbon-sphere composites	0.1 M HClO <sub>4</sub>	0.15	~0.50	~5.6	[4]
B,P,N-doped carbon	1 M HClO <sub>4</sub>	0.25	~0.65	~5.9	[11]
P, N-doped graphene	0.1 M HClO <sub>4</sub>	0.70	0.64	~3.5	[12]
N-doped carbon	0.50 M H <sub>2</sub> SO <sub>4</sub>	0.60	0.56	~4.9	[13]
Nitrogen-doped carbon xerogel	0.50 M H <sub>2</sub> SO <sub>4</sub>	0.38	~0.65	~5.2	[14]
Nitrogen-doped graphene/CNT	0.1 M HClO <sub>4</sub>	0.20	~0.55	~5.9	[15]
N-doped mesoporous carbon capsules with iron traces	0.50 M H <sub>2</sub> SO <sub>4</sub>	0.10	~0.55	~3.5	[16]
3D ordered mesoporous iron-nitrogen doped carbon material	0.1 M HClO <sub>4</sub>	0.40	~0.70	~5.6	[17]

**Note:** The ORR measurements were conducted in O<sub>2</sub>-saturated acid solution with the rotation speed of 1600 rpm, and all  $E_{1/2}$  values were versus RHE.

### 3. Computational Section

*Methods and Models.* First-Principles calculations were carried out within the density functional theory framework.<sup>18</sup> The projector-augmented wave (PAW) method<sup>19, 20</sup> and the generalized gradient approximation (GGA)<sup>21</sup> for the exchange-correlation energy functional, as implemented in the Vienna *ab initio* simulation package (VASP)<sup>22-24</sup> were used. The GGA calculation was performed with the Perdew-Burke-Ernzerhof (PBE)<sup>25</sup> exchange-correlation potential. A  $6 \times 6$  graphene supercell ( $14.89 \times 14.89$  Å) with vacuum length 12 Å was used for this work. A plane-wave cutoff energy of 400 eV was used. All atoms were fully relaxed with a tolerance in total energy of 0.01 meV, and the forces on each atom were less than 0.01 eV/Å.

The four electron pathway by which the ORR occurs under base condition are generally reported to proceed according to the following steps:<sup>26</sup>

- (1)  $\text{O}_2(\text{g}) + * \Rightarrow \text{O}_2^*$
- (2)  $\text{O}_2^* + \text{H}_2\text{O}(\text{l}) + \text{e}^- \Rightarrow \text{OOH}^* + \text{OH}^-$
- (3)  $\text{OOH}^* + \text{e}^- \Rightarrow \text{O}^* + \text{OH}^-$
- (4)  $\text{O}^* + \text{H}_2\text{O}(\text{l}) + \text{e}^- \Rightarrow \text{OH}^* + \text{OH}^-$
- (5)  $\text{OH}^* + \text{e}^- \Rightarrow \text{OH}^- + *$

To model the thermodynamics of the ORR, it is more convenient to work at alkaline conditions based on Nørskov's model.<sup>27</sup> Following the methodology developed by Nørskov *et. al.*, the chemical potential (the free energy per H) for the reaction ( $\text{H}^+ + \text{e}^-$ ) is equal to that of  $1/2 \text{H}_2$  by setting the reference potential to be that of the standard hydrogen electrode at standard condition (pH=0,  $P_{\text{H}_2}=1$  bar, and

T=298 K). As a result, the reaction free energy ( $\Delta G$ ) is further calculated by the formula:  $\Delta G = \Delta H - T\Delta S - qU + kBT\ln 10^*(pH)$ , where  $\Delta H$  is the reaction enthalpy of an elementary step in ORR and is estimated by the reaction energy ( $\Delta E$ ) from DFT calculations with zero-point energy (ZPE) correction;  $T\Delta S$  is the change in entropy contribution to the free energy;  $U$  is the applied potential;  $q$  is the charge transfer in each elementary step. Note that the energy (i.e. enthalpy) of  $H_2O(l)$  is approximately by that of  $H_2O(g)$  while the entropy of  $H_2O(l)$  to is calculated by  $S_{H_2O(g)} + \Delta S_{g-l}$ , where the entropy change from  $H_2O(g)$  to  $H_2O(l)$ ,  $\Delta S_{g-l}$  is chosen to be  $-118.9$  J/K/mol at 298 K, obtained from the ‘‘CRC Handbook of Chemistry and Physics’’.<sup>28</sup>

**Table S5.** Free energies of the Co-N<sub>4</sub>, Co-N<sub>3</sub>P, Co-N<sub>2</sub>P<sub>2</sub>, and Co-NP<sub>3</sub>-doped graphene materials in zigzag and armchair nanoribbons, respectively.

	<b>zigzag</b>	<b>armchair</b>
<b>Co-N<sub>4</sub></b>	-768.686	-727.095
<b>Co-N<sub>3</sub>P</b>	-766.126	-723.579
<b>Co-N<sub>2</sub>P<sub>2</sub></b>	-728.625	-695.804
<b>Co-NP<sub>3</sub></b>	-716.358	-658.293

**Table S6.** Reaction energetics for the 4-electron transfer processes during ORR.  $\Delta G$ , free energy change at T=298 K, pH=13 and U=0 V.

Elementary Reactions	Co-N <sub>3</sub> P/C	Co-N <sub>4</sub> /C
	$\Delta G$	$\Delta G$
$O_2(g) + * \Rightarrow O_2^*$	0	0
$O_2^* + H_2O(l) + e^- \Rightarrow OOH^* + OH^-$	0.042	0.85
$OOH^* + e^- \Rightarrow O^* + OH^-$	-0.958	-0.568
$O^* + H_2O(l) + e^- \Rightarrow OH^* + OH^-$	-1.171	-1.487
$OH^* + e^- \Rightarrow OH^- + *$	-1.588	-1.588

**Table S7.** Binding energies (eV) of adsorbates during oxygen reduction reaction on Co-N<sub>3</sub>P/C and Co-N<sub>4</sub>/C.

	Co-N <sub>3</sub> P/C	Co-N <sub>4</sub> /C
<b>O</b>	-2.453	-3.213
<b>O<sub>2</sub></b>	-0.682	-1.290
<b>OH</b>	-2.367	-3.015
<b>OOH</b>	-3.619	-3.802
<b>H<sub>2</sub>O</b>	-4.219	-4.643

**Table S8.** Frequencies (cm<sup>-1</sup>), zero point energies (ZPE) for different intermediates on Co-N<sub>3</sub>P/C and Co-N<sub>4</sub>/C.

	Frequencies (cm <sup>-1</sup> )	ZPE (eV)
<b>O*</b>	81.676722, 23.31557, 13.3725	0.0592
<b>OH*</b>	12.668964, 20.10811, 23.67828, 57.60446, 106.6064, 462.923	0.3418
<b>OOH*</b>	11.395939, 12.42573, 19.54492, 28.69787, 56.69379, 58.03127, 109.572, 165.5949, 427.4841	0.4449
<b>H<sub>2</sub>O</b>	365.715, 715, 953, 756	0.5584
<b>H<sub>2</sub></b>	4401	0.2728
<b>O<sub>2</sub></b>	1580	0.0979

#### 4. References

1. Newville, M. J. *Synchrotron Radiat.* 2001, 8, 322-324.
2. Y. Y. Li, F. Y. Cheng, J. N. Zhang, Z. M. Chen, Q. Xu and S. J. Guo, *Small* 2016, 12, 2839-2845.
3. X. C. Yan, Y. Jia, J. Chen, Z. H. Zhu and X. D. Yao, *Adv. Mater.* 2016, **28**, 8771-8778.
4. J. Wang, L. Q. Li, X. Chen, Y. L. Lu, W. S. Yang and X. Duan, *Nano Res.* 2017, **10**, 2508-2518.
5. P. Z. Chen, T. P. Zhou, L. L. Xing, K. Xu, Y. Tong, H. Xie, L. D. Zhang, W. S. Yan, W. S. Chu, C. Z. Wu and Y. Xie, *Angew. Chem. Int. Ed.* 2016, **55**, 1-6.

6. C. Tang, B. Wang, H.-F. Wang, and Q. Zhang, *Adv. Mater.* 2017, **29**, 1703185.
7. W. J. Jiang, L. Gu, L. Li, Y. Zhang, X. Zhang, L. J. Zhang, J. Q. Wang, J. S. Hu, Z. D. Wei and L. J. Wan, *J. Am. Chem. Soc.* 2016, **138**, 3570-3578.
8. Y. Zheng, Y. Jiao, Y. H. Zhu, Q. R. Cai, A. Vasileff, L. H. Li, Y. Han, Y. Chen and S. Z. Qiao, *J. Am. Chem. Soc.* 2017, **139**, 3336-3339.
9. B. Li, H. Nam, J. Zhao, J. Chang, N. Lingappan, F. Yao, T. H. Lee and Y. H. Lee, *Adv. Mater.* 2017, **29**, 1605083.
10. G. T. Fu, Z. Cui, Y. Chen, Y. Li, Y. Tang and J. B. Goodenough, *Adv. Energy Mater.* 2017, **7**, 1601172.
11. C. H. Choi, S. H. Park and S. I. Woo, *ACS Nano* 2012, **6**, 7084-7091.
12. C. H. Choi, M. W. Chung, H. C. Kwon, S. H. Park and S. I. Woo, *J. Mater. Chem. A* 2013, **1**, 3694-3699.
13. W. Wei, H. W. Liang, K. Parvez, X. D. Zhuang, X. L. Feng and K. Mullen, *Angew. Chem. Int. Ed.* 2014, **126**, 1596-1600.
14. H. Jin, H. M. Zhang, H. X. Zhong and J. L. Zhang, *Energy Environ. Sci.* 2011, **4**, 3389-3394.
15. J. L. Shui, M. Wang, F. Du and L. M. Dai, *Sci. Adv.* 2015, **1**, e1400129-e1400135.
16. G. A. Ferrero, K. Preuss, A. Marinovic, A. B. Jorge, N. Mansor, D. J. Brett, A. B. Fuertes, M. Sevilla and M. M. Titirici, *ACS Nano* 2016, **10**, 5922-5932.
17. H. B. Tan, Y. Q. Li, X. F. Jiang, J. Tang, Z. L. Wang, H. Y. Qian, P. Mei, V. Malgras, Y. Bando and Y. Yamauchi, *Nano Energy* 2017, **36**, 286-294.

18. W. Kohn and L. J. Sham, *Phys. Rev.* 1965, **140**, A1133-A1138.
19. P. E. Blöchl, *Phys. Rev. B* 1994, **50**, 17953-17979.
20. G. Kress and D. Joubert, *Phys. Rev. B* 1999, **59**, 1758-1775.
21. J. P. Perdew and Y. Wang, *Phys. Rev. B* 1992, **45**, 13244-13249.
22. G. Kresse and J. Hafner, *Phys. Rev. B* 1993, **47**, 558-561.
23. G. Kresse and J. Furthmuller, *Phys. Rev. B* 1996, **54**, 11169-11186.
24. G. Kresse and J. Furthmuller, *Comput. Mater. Sci.* 1996, **6**, 15-50.
25. J. P. Perdew, K. Burke and M. Ernzerhof, *Phys. Rev. Lett.* 1996, **77**, 3865-3868.
26. Y. Jiao, Y. Zheng, M. Jaroniec and S. Z. Qiao, *Chem. Soc. Rev.* 2015, **44**, 2060-2086.
27. J. K. Nørskov, J. Rossmeisl, A. Logadottir, L. Lindqvist, J. R. Kitchin, T. Bligaard and H. Jo'nsson, *J. Phys. Chem. B* 2004, **108**, 17886-17892.
28. W. M. Haynes, *CRC Handbook of Chemistry and Physics*, CRC Press, Boca Raton, 2005.